

EDGE ARTICLE

View Article Online
View Journal | View IssueCite this: *Chem. Sci.*, 2021, **12**, 14540

All publication charges for this article have been paid for by the Royal Society of Chemistry

Received 22nd July 2021
Accepted 7th October 2021

DOI: 10.1039/d1sc04018a

rsc.li/chemical-science

Single entity measurements have been introduced by Bard and Wightman based on the collisions/reactions of individual nanoparticles and molecules at an ultramicroelectrode (UME).^{1–9} Since then, the field of single entity electrochemistry has gradually attracted several research groups and has become a frontier field of nanoelectrochemistry and electroanalytical chemistry.^{8,10–14} For instance, it has been shown that the chemistry of the electrode surface plays an important role in the collision/reaction events and the kinetics of reaction processes.^{15–21} Dasari *et al.* reported that hydrazine oxidation and proton reduction can be detected using single Pt nanoparticles on the surface of a mercury or bismuth modified Pt UME, and the material of the electrode was found to affect the shape of current-time transients.^{22,23} Fast scan cyclic voltammetry provides better chemical information about transient electrode–nanoparticle interactions, which is otherwise difficult to obtain with constant-potential techniques.²⁴ There are only a few reports on photoelectrochemical systems including semiconductor nanoparticles designed to detect single nanoparticles in the course of photocatalysis processes.^{25–28} More importantly, owing to the nature of stochastic processes of single entity reactions, statistical analyses have shown substantial influences on the understanding of the underlying processes.

Electrochemiluminescence or electrogenerated chemiluminescence (ECL),²⁹ as a background-free technique,^{30–32} was also utilized to detect individual chemical reactions and single Pt nanoparticle collisions based on the reaction between the Ru(bpy)₃²⁺ complex and tri-*n*-propylamine (TPrA) radicals on the surface of an ITO electrode.^{2,33,34} It was found that the size of the

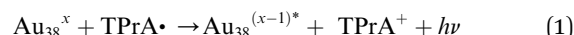
Monitoring single Au₃₈ nanocluster reactions via electrochemiluminescence†

Mahdi Hesari, ^a Hui Ma ^{*b} and Zhifeng Ding ^{*a}

Herein, we report for the first time single Au₃₈ nanocluster reaction events of highly efficient electrochemiluminescence (ECL) with tri-*n*-propylamine radicals as a reductive co-reactant at the surface of an ultramicroelectrode (UME). The statistical analyses of individual reactions confirm stochastic single ones influenced by the applied potential.

nanoparticles, the origin of the interaction between particles and the electrode surface, the concentration of species generation, and the lifetime of individual electrogenerated nanocluster species (*i.e.*, Au₃₈²⁺, Au₃₈³⁺, and Au₃₈⁴⁺) in conjunction with the reactivity of those oxidized species with co-reactant radical intermediates (*i.e.*, TPrA radical) play crucial roles in the frequency of the ECL reaction events leading to individual ECL responses. More strikingly, a higher ECL reaction frequency is directly proportional to the amount of collected ECL light.²¹ Chen and co-workers also employed ECL to study stationary single gold–platinum nanoparticle reactivity on the surface of an ITO electrode.³⁵ Lin and co-workers monitored the hydrogen evolution reaction in the course of “ON” and “OFF” ECL signals.³⁶ Recently, we performed a systematic and mechanistic ECL study of a series of gold nanoclusters, with the general formula of Au_{*n*}(SC₂H₄Ph)_{*m*}^{*z*} (*n* = 25, 38, 144, *m* = 18, 24, 60 and *z* = −1, 0, +1), where near-infrared (NIR) ECL emission was observed.³⁷ There are several enhancement factors, such as catalytic loops^{38,39} that improve the signal to noise ratio. The Wightman group was able to report single ECL reactions based on the capability of ECL.⁷ Furthermore, thus far, we have explored ECL mechanisms and reported the ECL efficiency of five different gold nanoclusters *i.e.*, Au₂₅(SR)₁₈^{−1}, Au₂₅(SR)₁₈⁰, Au₂₅(SR)₁₈¹⁺, Au₃₈(SR)₂₄⁰ and Au₁₄₄(SR)₆₀⁰, among which the Au₃₈(SR)₂₄⁰/TPrA system revealed outstanding ECL efficiency, *ca.* 3.5 times higher than that of Ru(bpy)₃²⁺/TPrA as a gold standard. Therefore, we decided to focus on the Au₃₈(SR)₂₄⁰/TPrA system. It was discovered that the ECL emission of these nanomaterials can be tuned through varying the applied potential and local concentration of the desired co-reactant.

Herein, for the first time we report on ECL *via* a single Au₃₈(SC₂H₄Ph)₂₄ nanocluster (hereafter denoted as Au₃₈ NC) reaction (eq. (1)) in the vicinity of an UME in the presence of TPrA radicals as a reductive co-reactant.



where *x* is the oxidation number that can be either 0, 1, 2, 3 or 4. Single ECL spikes (Fig. 1A) along with ECL spectroscopy were

^aDepartment of Chemistry, The University of Western Ontario, London, Ontario N6A 5B7, Canada. E-mail: zfding@uwo.ca

^bState Key Laboratory of Analytical Chemistry for Life Science, School of Chemistry and Chemical Engineering, Nanjing University, Nanjing 210023, China. E-mail: mahui@nju.edu.cn

† Electronic supplementary information (ESI) available. See DOI: 10.1039/d1sc04018a



used for elucidating individual reaction events. Indeed, each single ECL spike demonstrates a single $\text{Au}_{38}^{(x-1)*}$ reaction product. Au_{38} NCs were synthesized according to procedures reported by us and others, and fully characterized using UV-Visible-NIR, photoluminescence, ^1H NMR spectroscopy and MALDI mass spectrometry to confirm the Au_{38} nanocluster synthesis (details are provided in ESI, Sections 1–3, Fig. S1–S4†).^{38,40,41} Fig. 2 (left) shows a differential pulse voltammogram (DPV) in an anodic scan of a 2 mm Pt disc electrode immersed in 0.1 mM Au_{38} acetonitrile/benzene solution containing 0.1 M TBAPF₆ as the supporting electrolyte. There are five discrete electrochemical peaks at which Au_{38}^0 was oxidized to Au_{38}^{+} ($E^\circ = 0.39$ V), Au_{38}^{2+} ($E^\circ = 0.60$ V), and $\text{Au}_{38}^{3+/4+}$ ($E^\circ = 0.99$ V) and reduced to Au_{38}^{-} ($E^\circ = -0.76$ V) and Au_{38}^{2-} ($E^\circ = -1.01$ V).^{38,40,41}

The rich electrochemistry of Au_{38} NCs is well-matched with that of co-reactants such as TPrA to generate near infrared-ECL (NIR-ECL), and the ECL emission efficiency of the Au_{38} /TPrA system is 3.5 times larger than that of the $\text{Ru}(\text{bpy})_3^{2+}$ /TPrA co-reactant ECL system.²⁷

Thus, it is of utmost interest to investigate the ECL generation of the above co-reactant system in single reactions, which improves the ECL signal detection sensitivity. To perform the ECL experiment a solution of 10 μM Au_{38} NC with 20 mM TPrA was prepared. We first confirmed the ECL light generation of such solution along with its blank solution containing only TPrA using a typical 2 mm diameter Pt disk electrode (Fig. 2, S5 and S6†).

A 10 μm Pt UME electrode, which is electrochemically inert (Fig. S7†), was utilized to investigate the ECL of single NC reactions under potentiostatic conditions, at which a specific positive bias potential was applied to oxidize both Au_{38} and TPrA. Fig. 1A shows a typical ECL–time transient current curve (ECL intensity *versus* time) at 0.90 V *vs.* SCE, which was acquired

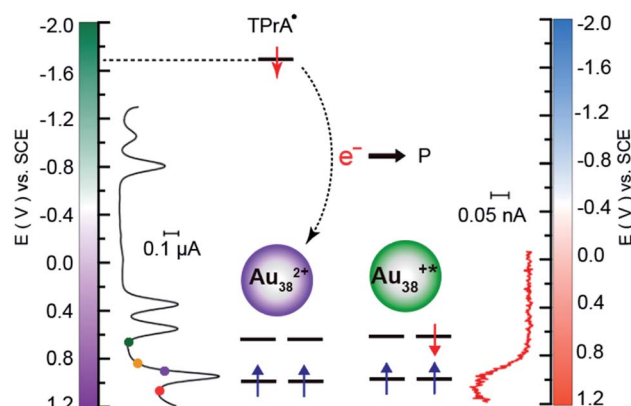


Fig. 2 Anodic DPV for Au_{38} (left), reaction energy diagram of Au_{38}^{2+} and TPrA^\cdot (middle) along with the ECL–voltage curve (right) in an anodic potential scan at a 2 mm Pt disk electrode immersed in a solution of 10 μM Au_{38} with 20 mM TPrA.

using a photomultiplier tube (PMT, R928) for a duration of 1800 s at data acquisition time intervals of 15 ms (Fig. 1C and ESI, Section 3†). Fig. 1B represents an exemplary event of a single ECL spike with a sharp increase followed by a decay in the ECL intensity. It is observed from the many spikes in Fig. 1B that this process can reoccur with a high probability in the vicinity of the UME, probably due to an electrocatalytic reaction loop (Fig. 1C). Indeed, ECL intensity was enhanced in this way as an already relaxed species, *i.e.*, Au_{38}^{z+1*} , participates in an oxidation step to regenerate Au_{38}^{z+1} to react with the TPrA radical (TPrA^\cdot).

Once photons resulting from the excited state relaxation in the vicinity of the UME are captured by the PMT, individual reaction events can be observed (Fig. 1A with the instrumentation schematic shown in Fig. 3C). As shown in Fig. 3A, there are

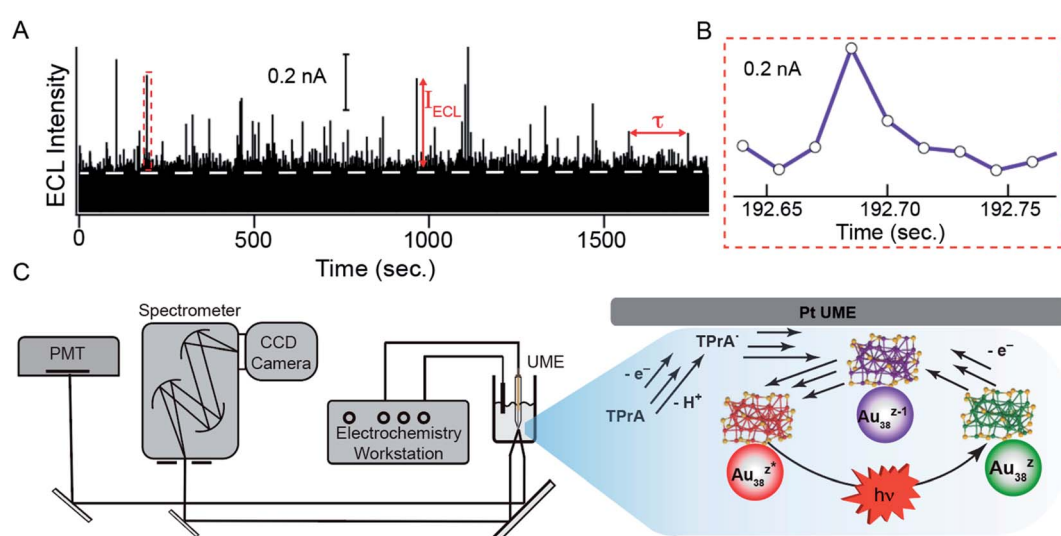


Fig. 1 (A) An example of the reaction event transient of 10 μM Au_{38} in benzene/acetonitrile (1 : 1) containing 0.1 M TBAPF₆ in the presence of 20 mM TPrA at 0.9 V *vs.* SCE, acquired at 15 ms time intervals using a 10 μm Pt UME. The white dashed-line indicates the threshold to identify single ECL spikes. (B) Illustration of a single nanocluster ECL spike. (C) ECL instrumentation with an inset showing ECL spike generation in the vicinity of the Pt UME.



many ECL spikes during 1800 s of measurement, each of which represents an individual ECL generation reaction in the vicinity of the UME surface. It is worth noting that there are several spikes with various intensities. This is most likely due to the Brownian motion which is random movement due to the diffusion of individual nanocluster species such as Au_{38}^0 , Au_{38}^{1+} , Au_{38}^{2+} , etc., electrogenerated at the local applied potentials. Long and co-workers⁴² proposed that silver nanoparticle collision on the surface of a gold electrode follows Brownian motion, leading to several types of surface-nanoparticle response peak shapes. In fact, the observed ECL spikes, shown in Fig. 1C, with a rise and an exponential decay suggested that Au_{38} nanocluster species diffuse directly through the electrode double-layer, move towards the tunneling region of the electrode surface, collide⁴² and become oxidized, react with TPrA radicals thereafter to produce excited states, and emit ECL. It is worth emphasizing that this path could be partially different for each individual nanocluster owing to the angle and direction relative to the electrode surface. The single Au_{38} NC reaction behaviour at various bias potentials was investigated following the electrochemical energy diagram shown in Fig. 2, middle. For example, at a bias potential of 0.70 V (the green spot on the DPV in Fig. 2), Au_{38}^0 undergoes two successive oxidation

reactions to Au_{38}^{2+} and TPrA oxidation and deprotonation start to generate TPrA \cdot . In fact, at a very close oxidation potential to Au_{38}^{2+} , TPrA is also oxidized to its corresponding cation radical (*ca.* 0.80 V vs. SCE) Fig. S6,[†] followed by deprotonation to form the TPrA radical.³⁸ The TPrA \cdot with a very high reduction power ($E^{\circ'} = -1.7$ eV)⁴³ injects one electron to the LUMO orbital of the nanocluster and forms excited state Au_{38}^{2+*} , as illustrated in the reaction energy diagram in Fig. 2, middle.³⁸ Then, Au_{38}^{2+*} emits ECL light while relaxing to the ground state. For another instance, at 1.10 V vs. SCE (the red spot on the DPV in Fig. 2), Au_{38}^0 is oxidized to $\text{Au}_{38}^{3/4+}$ feasibly. At this potential, the TPrA radical is generated massively in the vicinity of the electrode. The efficient electron transfer between the TPrA radical and $\text{Au}_{38}^{3/4+}$ generates both Au_{38}^{2+*} and Au_{38}^{3+*} that emit light at the same wavelength of 930 nm.³⁸ The results of such interactions produced a transient composed of many ECL events (Fig. 3A), which is an indication of bias potential enforcement on the nanocluster light emission.

We further tried to collect the current-time traces of such events; however, owing to the high background current originating from the high concentration of TPrA relative to that of the nanocluster, no noticeable spikes in the current were observed.

In order to study the photochemistry and understand deeply the single nanocluster reactions, ECL-time transients were collected at different applied potentials (*i.e.*, 0.7, 0.8, 0.9 and 1.1 V vs. SCE) as labelled in green, brown, purple, and red on the DPV in Fig. 2, respectively. The transients were further analysed using our home-written MATLAB algorithm adapted from that for nanopore electrochemistry.⁴⁴ The population of individual events was identified by applying an appropriate threshold to discriminate ECL spikes from the noise as demonstrated in Fig. 1A. In fact, the applied algorithm also assisted us to learn about the raising time and intensity of each spike, as well as photons of individual spikes. For instance, Fig. 3A shows another typical transit for 1800 s at an UME potential bias of 1.1 V for the ECL events. Indeed, the integrated area of each peak, the charge of the photoelectrons at the PMT, is directly proportional to the number of photons emitted from individual reactions (see ESI, Section 5[†]). Basically, the PMT amplifies the collected single photon emitted in the course of light-to-photoelectron conversion (see ESI, Section 6 and Fig. S8[†]) and translates a single photon into photoelectrons. The extracted charge of each ECL reaction, Q_{ECL} , was then converted to the corresponding number of photons by dividing by the gain factor, g , which is 1.55×10^6 (Fig. S8[†]), following eqn (2):

$$\text{number of photons} = \frac{Q_{\text{ECL}}}{g} \quad (2)$$

The histograms of the number of photons show a Gaussian distribution (Fig. 3B) with a reaction frequency of 53.5 ± 2.9 at $E = 1.1$ V, whereas at a lower potential of 0.7 V the reaction frequency drops to 18.5 ± 1.7 (Fig. 3F). This indicates that there is a three-fold lower reaction occurrence at the lower potential. The integration of the Gaussian fitting at 1.1 V and 0.7 V also

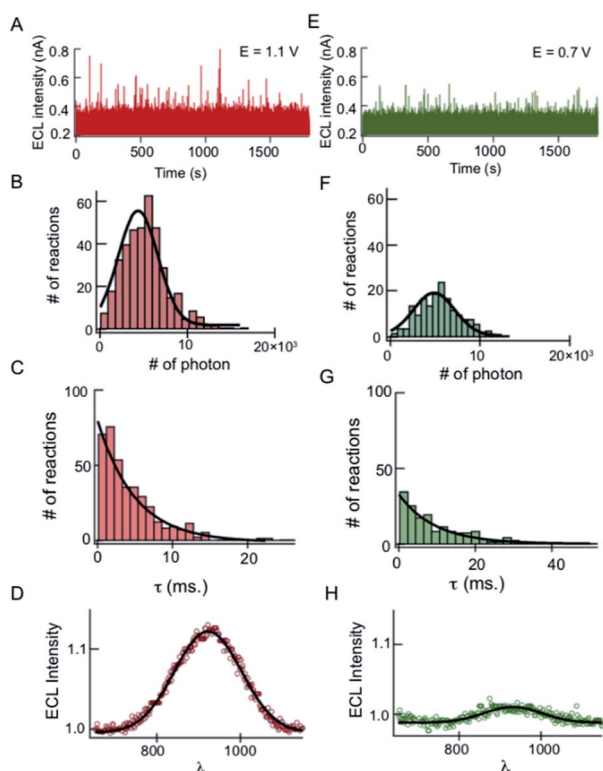


Fig. 3 Single-nanocluster ECL photoelectron spectroscopy of Au_{38} . ECL-time transients (A), statistics of the number of photons (B), histogram of the single reaction time between sequential spikes (C) and accumulated ECL spectrum (D) for a 10 μm Pt UME at 1.1 V immersed in a 10 μM Au_{38} nanocluster solution in benzene/acetonitrile (1 : 1) containing 0.1 M TBAPF₆ in the presence of 20 mM TPrA. (E)–(H) The counterpart plots to (A)–(D) for the UME biased at 0.7 V. # represents the number.



reveals a three-fold drop from 3.3×10^5 to 1.2×10^5 photons over 1800 s.

To further explore the effect of electrode potential bias on the single Au_{38} NCs ECL reaction, potentials lower than 1.1 and higher than 0.7 V, *ca.* 0.8 and 0.9 V (brown and purple labels in Fig. 2), were applied. In fact, the resulting ECL-time transients show a lower population of single spikes (Fig. S12A and ESI,†). The integrated Gaussian curve values support the ECL-time transient observations with $\sim 4.1 \times 10^4$ and $\sim 6.5 \times 10^4$ photons, respectively. In fact, it is unlikely that the PMT would get more than two events in the duration, owing to the following reasons: (i) it has been shown that only 5.5% of incoming photons can be effectively converted to photoelectron signals by our R928 PMT during our absolute efficiency calibration, ESI Section 6 and Fig. S8–S19†;⁴⁵ (ii) spherical ECL emission is proven to be detected for a substantial small part upon examination of our detection system for the absolute ECL quantum efficiency;⁴⁵ (iii) Au_{38} nanocluster ECL emissions occur at 930 nm, which is almost at the wavelength detection limit of our PMT response curve.^{38,45}

In addition, we evaluated the stochastic (a series of random events at various probability distributions) nature of the observed events and extracted the reaction time interval (τ) at various potentials. The resulting graph shows an exponential decay (Fig. 3C) as expressed in eqn (3):

$$f(t) = A \exp^{-\lambda t} \quad (3)$$

where frequency (λ) gives the mean rate of the event and A represents the fitting amplitude. One can expect to obtain the distribution of the number of emitted photons and spatial brightness function. In fact, the exponential decay is a clear indication of random single reaction events as Whiteman and co-workers described for a 9,10-diphenylanthracene (DPA) ECL system in the annihilation pathway.^{7,46} At a potential of 1.1 V, λ and A are found to be $4.98 \pm 0.02 \text{ ms}^{-1}$ and 80.4 ± 3.2 , whereas at 0.7 V, λ and A turned out to be $32.9 \pm 1.6 \text{ ms}^{-1}$ and 9.5 ± 0.1 (Fig. 3C and G). Indeed, the lower potential of 0.70 V *vs.* SCE is high enough to generate the TPrA radical along with Au_{38}^{2+} , thereby leading to excited Au_{38}^{+*} , Fig. 3E. One can conclude that at the applied potentials of 0.7 V and 1.1 V, Au_{38}^0 is oxidized to Au_{38}^{2+} and Au_{38}^{4+} , resulting in the generation of Au_{38}^{+*} and Au_{38}^{3+*} under static conditions. Thus, there are higher populations of ECL spikes with no discrepancy in the number of collected photon distributions. However, at two intermediate potentials, *i.e.*, 0.8 and 0.9 V, a dynamic behaviour which is due to the mixed oxidation of Au_{38} species, in the vicinity of the UME, is observed. In fact, at these two applied potentials, the local concentration of the corresponding gold nanoclusters (*i.e.*, Au_{38}^{3+} and Au_{38}^{4+}) is not sufficient to produce significant ECL spikes. We also attempted to collect the ECL spectrum using a charge-coupled device (CCD) camera, which is relatively more sensitive in the NIR region (*e.g.*, $\lambda > 900 \text{ nm}$, Fig. S16†). Fig. 3D and H display an accumulated spectrum at 1.1 and 0.7 V *vs.* SCE, which is collected for 30 minutes. The fitted accumulated ECL spectrum indicates an ECL peak emission at 930 nm and supports higher reactivity at 1.1 V than that at 0.7 V.³⁸ To confirm that the observed ECL spikes and accumulated spectra

are generated based on the oxidation of Au_{38} nanoclusters in the presence of TPrA radicals, ECL-time transients were recorded upon holding an applied potential at which no faradaic process occurs. Fig. S11† represents ECL-time curves and accumulated ECL spectra at 0.0 V and 0.4 V. One can notice that no appreciable ECL signal can be observed.

In addition, we investigate the Pearson cross-correlation (ρ) between the intensities of ECL spikes with τ as shown in Fig. S14† in which there is a positive correlation at 0.7 and 1.0 V and a negative correlation at 0.8 and 0.9 V. In fact, ρ evaluates whether there is a stationary random process between the two defined parameters (see ESI, Section 6†). Interestingly, the frequency of the reaction at different applied potentials revealed decay from 0.7 to 0.8 V, followed by an upward trend to 0.9 and 1.1 V *vs.* SCE (Fig. S15†). This could be additional support for the transition stage at 0.8 and 0.9 V, where the applied potential as the major driving force to generate oxidized forms (*e.g.*, Au_{38}^{3+} and Au_{38}^{4+}) governs the flux of the nanocluster species that reach the vicinity of the electrode. Furthermore, the effectiveness of electron transfer reaction kinetics between the radical species, *i.e.*, Au_{38}^{z+1} and TPrA radical, competes with the flow of the incoming nanoclusters. It is worth mentioning that each of the ECL single event experiments was repeated three times, and very similar results were obtained. Moreover, lower (5 μM) and higher (20 μM) concentrations of Au_{38} in the presence of 20 mM were tested. In fact, the former shows a smaller number of single reactions; however the later revealed a larger number of multiple reactions (Fig. S13†).

In summary, in this communication we demonstrated that Au_{38} NC ECL at the single reaction level can be monitored using a simple photoelectrochemical setup following a straightforward protocol. Indeed, we have rich basic knowledge about the ECL mechanisms of various gold nanoclusters with different charge states ($\text{Au}_{25}(\text{SR})_{18}^{1+}$, $\text{Au}_{25}(\text{SR})_{18}^0$, $\text{Au}_{25}(\text{SR})_{18}^{1-}$) and various sizes ($\text{Au}_{25}(\text{SR})_{18}^0$, $\text{Au}_{38}(\text{SR})_{24}^0$, $\text{Au}_{144}(\text{SR})_{60}^0$) in fine detail. Thus, the ECL emission mechanisms of gold clusters, including the contribution of each charge state and influence of various concentrations of co-reactants, are well known. For instance, in our previous studies^{38,39,47–49} we clearly identified three charge states of an $\text{Au}_{25}(\text{SR})_{18}^{1-}$ /TPrA system and we discovered that at a high concentration of TPrA the reduction in the bulk solution of gold nanoclusters influences the ECL emission wavelength. We also have learnt that the Au_{38} /TPrA system is a co-reactant independent of co-reactant concentration. Furthermore, an extensively higher concentration of TPrA provides a dominant reaction over any unknown decomposition reaction at higher oxidation states of Au_{38} . It was discovered that the population of ECL reactions is directly governed by the applied bias potential on a Pt UME. This work is a strong indication of the high sensitivity of the ECL technique in detecting single ECL reactions in a simple solution, which complements those reported by the Bard group using rubrene, for instance, embedded in an organic emulsion in the presence of TPrA or oxalate as a co-reactant.^{50,51} These systems needed a substantial ECL enhancement in the presence of an ionic liquid as the supporting electrolyte and emulsifier. The current approach can be further extended to investigate other



molecules and nanomaterials' electrocatalytic processes at the single reaction level.

Data availability

Extra experimental results associated to this manuscript are available in the ESI.†

Author contributions

M. H., and Z. D. designed the experiment. M. H. performed synthesis, ECL experiments, and data analysis. H. M. analysed the data. M. H. and Z. D. wrote the manuscript. M. H., H. M., and Z. D. revised the manuscript.

Conflicts of interest

There are no conflicts to declare.

Acknowledgements

We thank the Department of Chemistry, Electronic Shop in Chemistry and ChemBioStores at The University of Western Ontario. We also thank Natural Sciences and Engineering Research Council of Canada (NSERC, DG RGPIN-2018-06556 and SPG STPGP-2016-493924) and the Natural Science Foundation of China (22104052) for the financial support to this research.

References

- 1 F.-R. F. Fan and A. J. Bard, *Science*, 1995, **267**, 871–874.
- 2 F.-R. F. Fan and A. J. Bard, *Nano Lett.*, 2008, **8**, 1746–1749.
- 3 X. Xiao and A. J. Bard, *J. Am. Chem. Soc.*, 2007, **129**, 9610–9612.
- 4 X. Xiao, F.-R. F. Fan, J. Zhou and A. J. Bard, *J. Am. Chem. Soc.*, 2008, **130**, 16669–16677.
- 5 F.-R. F. Fan, J. Kwak and A. J. Bard, *J. Am. Chem. Soc.*, 1996, **118**, 9669–9675.
- 6 A. J. Bard and F.-R. F. Fan, *Acc. Chem. Res.*, 1996, **29**, 572–578.
- 7 M. M. Collinson and R. M. Wightman, *Science*, 1995, **268**, 1883–1885.
- 8 H. Ren and M. A. Edwards, *Curr. Opin. Electrochem.*, 2021, **25**, 100632.
- 9 F.-R. F. Fan, S. Park, Y. Zhu, R. S. Ruoff and A. J. Bard, *J. Am. Chem. Soc.*, 2009, **131**, 937–939.
- 10 W. Zhao, H.-Y. Chen and J.-J. Xu, *Chem. Sci.*, 2021, **12**, 5720–5736.
- 11 S. D. Minteer, *J. Am. Chem. Soc.*, 2018, **140**, 2701–2703.
- 12 Y. Fan, T. J. Anderson and B. Zhang, *Curr. Opin. Electrochem.*, 2018, **7**, 81–86.
- 13 L. A. Baker, *J. Am. Chem. Soc.*, 2018, **140**, 15549–15559.
- 14 S. M. Oja, M. Wood and B. Zhang, *Anal. Chem.*, 2012, **85**, 473–486.
- 15 C.-H. Chen, E. R. Ravenhill, D. Momotenko, Y.-R. Kim, S. C. S. Lai and P. R. Unwin, *Langmuir*, 2015, **31**, 11932–11942.
- 16 A. D. Castañeda, T. M. Alligrant, J. A. Loussaert and R. M. Crooks, *Langmuir*, 2015, **31**, 876–885.
- 17 X. Xiao, S. Pan, J. S. Jang, F.-R. F. Fan and A. J. Bard, *J. Phys. Chem. C*, 2009, **113**, 14978–14982.
- 18 A. Kaliyaraj Selva Kumar, R. Miao, D. Li and R. G. Compton, *Chem. Sci.*, 2021, **12**, 10878–10882.
- 19 B. Roehrich and L. Sepunaru, *Angew. Chem., Int. Ed.*, 2020, **59**, 19184–19192.
- 20 S.-M. Lu, J.-F. Chen, Y.-Y. Peng, W. Ma, H. Ma, H.-F. Wang, P. Hu and Y.-T. Long, *J. Am. Chem. Soc.*, 2021, **143**, 12428–12432.
- 21 H. Ma, J.-F. Chen, H.-F. Wang, P.-J. Hu, W. Ma and Y.-T. Long, *Nat. Commun.*, 2020, **11**, 2307.
- 22 R. Dasari, B. Walther, D. A. Robinson and K. J. Stevenson, *Langmuir*, 2013, **29**, 15100–15106.
- 23 R. Dasari, K. Tai, D. A. Robinson and K. J. Stevenson, *ACS Nano*, 2014, **8**, 4539–4546.
- 24 Z. Guo, S. J. Percival and B. Zhang, *J. Am. Chem. Soc.*, 2014, **136**, 8879–8882.
- 25 A. Fernando, S. Parajuli and M. A. Alpuche-Aviles, *J. Am. Chem. Soc.*, 2013, **135**, 10894–10897.
- 26 H. Tian, Y.-Y. Peng, H. Ma, W. Ma and Y.-T. Long, *Angew. Chem., Int. Ed.*, 2018, **57**, 3758–3762.
- 27 H. Ma, W. Ma, J.-F. Chen, X.-Y. Liu, Y.-Y. Peng, Z.-Y. Yang, H. Tian and Y.-T. Long, *J. Am. Chem. Soc.*, 2018, **140**, 5272–5279.
- 28 H. Ma, U. K. Gosh, Y.-L. Ying and Y.-T. Long, *ChemElectroChem*, 2021, **8**, 3221–3228.
- 29 M. Hesari and Z. Ding, *J. Electrochem. Soc.*, 2016, **163**, H3116–H3131.
- 30 J. Zhang, S. Arbault, N. Sojic and D. Jiang, *Ann. Rev. Anal. Chem.*, 2019, **12**, 275–295.
- 31 M. Sentic, S. Arbault, L. Bouffier, D. Manojlovic, A. Kuhn and N. Sojic, *Chem. Sci.*, 2015, **6**, 4433–4437.
- 32 S. Voci, B. Goudeau, G. Valenti, A. Lesch, M. Jović, S. Rapino, F. Paolucci, S. Arbault and N. Sojic, *J. Am. Chem. Soc.*, 2018, **140**, 14753–14760.
- 33 A. Fiorani, D. Han, D. Jiang, D. Fang, F. Paolucci, N. Sojic and G. Valenti, *Chem. Sci.*, 2020, **11**, 10496–10500.
- 34 L. Benoit and J.-P. Choi, *ChemElectroChem*, 2017, **4**, 1573–1586.
- 35 M.-J. Zhu, J.-B. Pan, Z.-Q. Wu, X.-Y. Gao, W. Zhao, X.-H. Xia, J.-J. Xu and H.-Y. Chen, *Angew. Chem., Int. Ed.*, 2018, **57**, 4010–1014.
- 36 C. Ma, H.-F. Wei, M.-X. Wang, S. Wu, Y.-C. Chang, J. Zhang, L.-P. Jiang, W. Zhu, Z. Chen and Y. Lin, *Nano Lett.*, 2020, **20**, 5008–5016.
- 37 M. Hesari and Z. Ding, *Acc. Chem. Res.*, 2017, **50**, 218–230.
- 38 M. Hesari, M. S. Workentin and Z. Ding, *ACS Nano*, 2014, **8**, 8543–8553.
- 39 M. Hesari, M. S. Workentin and Z. Ding, *Chem. Eur. J.*, 2014, **20**, 15116–15121.
- 40 H. Qian, Y. Zhu and R. Jin, *ACS Nano*, 2009, **3**, 3795–3803.
- 41 O. Toikkanen, V. Ruiz, G. Rönnholm, N. Kalkkinen, P. Liljeroth and B. M. Quinn, *J. Am. Chem. Soc.*, 2008, **130**, 11049–11055.



42 W. Ma, H. Ma, J.-F. Chen, Y.-Y. Peng, Z.-Y. Yang, H.-F. Wang, Y.-L. Ying, H. Tian and Y.-T. Long, *Chem. Sci.*, 2017, **8**, 1854–1861.

43 R. Y. Lai and A. J. Bard, *J. Phys. Chem. A*, 2003, **107**, 3335–3340.

44 Z. Gu, Y.-L. Ying, C. Cao, P. He and Y.-T. Long, *Anal. Chem.*, 2015, **87**, 907–913.

45 J. R. Adsetts, K. Chu, M. Hesari, J. Ma and Z. Ding, *Anal. Chem.*, 2021, **93**, 11626–11633.

46 N. G. Van Kampen, *Stochastic Processes in Physics and Chemistry*, Elsevier Science, 2011.

47 M. Hesari, Z. Ding and M. S. Workentin, *Organometallics*, 2014, **33**, 4888–4892.

48 M. Hesari, M. S. Workentin and Z. Ding, *RSC Adv.*, 2014, **4**, 29559–29562.

49 M. Hesari, M. S. Workentin and Z. Ding, *Chem. Sci.*, 2014, **5**, 3814–3822.

50 J. E. Dick, C. Renault, B.-K. Kim and A. J. Bard, *Angew. Chem. Int. Ed.*, 2014, **53**, 11859–11862.

51 J. E. Dick, C. Renault, B.-K. Kim and A. J. Bard, *J. Am. Chem. Soc.*, 2014, **136**, 13546–13549.

